2822 *Chem. Mater.* **2010,** *22,* 2822–2828
DOI:10.1021/cm903754k

CHEMISTRY OF MATERIALS
Article

Latex-Templated Silica Films: Tailoring Porosity to Get a Stable Low-Refractive Index

F. Guillemot,[†,‡,§,⊥] A. Brunet-Bruneau,[§] E. Bourgeat-Lami,[⊥] T. Gacoin,[†] E. Barthel,[‡] and J.-P. Boilot*[,†]

[†]*Groupe de Chimie du Solide, Laboratoire de Physique de la Matière Condensée, UMR CNRS 7643, Ecole Polytechnique, 91128 Palaiseau, France,* [‡]*Surface du Verre et Interfaces (CNRS/Saint-Gobain) UMR 125, 39 quai Lucien Lefranc, F-93303, Aubervilliers, France,* [§]*Institut des Nanosciences de Paris, UMR 7601, Université Paris 6, Campus Boucicaut, 140 rue de Lourmel, case 80, 75015 Paris, France, and* [⊥]*Laboratoire de Chimie, Catalyse, Polymères et Procédés (C2P2), UMR 5265 Université Lyon 1, CPE Lyon, CNRS, Bâtiment 308 F, 43 boulevard du 11 novembre 1918, BP 2077, 69616 Villeurbanne Cedex, France*

Received December 14, 2009. Revised Manuscript Received March 19, 2010

Porous sol−gel silica films are prepared using different PMMA latex nanoparticles, 30−80 nm in diameter, as sacrificial templates. By changing the size and the content of the latex particles in the deposited silica sol, it was possible for the first time to tailor the porosity of the sol−gel films (uniform pore size and porous fraction from 0.10 to 0.74) independently of their thickness. This is the consequence of a low microporosity in the silica walls as shown by the correspondence between the measured porous fraction after calcination and the starting latex volume fraction. No ethanol capillary condensation occurs in these films before high partial pressure (above 0.9), leading to a stable refractive index that can be tuned in a large range (from 1.15 to 1.40 at 600 nm). A porosity percolation transition with the opening of the extrinsic pore interconnection was observed at a pore fraction threshold of about 0.40 for different sizes of the initial template. Below the threshold, the films showed a closed porosity structure with a low stable refractive index (down to 1.29 at 600 nm), opening the way to their use for antireflective applications.

Introduction

Integrated optical devices are demanding the development of reliable low refractive index materials.[1] Especially, thin films with a low refractive index ($n < 1.30$, low-n) are effective in improving the performance of antireflective coatings, which are widely used on solar cells, eyeglasses, computer monitors, and any other optical surface that needs to weaken the reflectance and improve the optical quality of images.

One of the most suitable material for low-n applications is silica as its polarizability in the bulk state is relatively low (n (600 nm) = 1.458).[2] Low-n silica films have been prepared through various approaches.[2−5] Compared to more traditional coating techniques (like CVD and sputtering),[6−11] the potential of sol−gel-derived coatings has been clearly shown because the sol−gel thin film processing permits to independently tailor the chemical composition and the microstructure of the deposited films, through the use of a sacrificial template,[12−19] or by the deposition of silica in a colloidal state.[5]

A now well developed approach to prepare porous sol−gel silica films consists in creating porosity through the use of sacrificial organic templates (called porogens) that are removed during film curing at typically 250−450 °C.

*Corresponding author. Tel.: (33)-1- 69 33 46 51. Fax: (33)-1- 69 33 47 99. E-mail: jean-pierre.boilot@polytechnique.edu.

(1) Chen, D. *Sol. Energy Mater. Sol. Cells* **2001**, *68*, 313–336.
(2) Maex, K.; Baklanov, M. R.; Shamiryan, D.; Iacopi, F.; Brongersma, S. H.; Yanovitskaya, Z. S. *J. Appl. Phys.* **2003**, *93*, 8793–8841.
(3) Pettit, R. B.; Ashley, C. S.; Reed, S. T.; Brinker, C. J. In *Sol-Gel Technology For Thin Films, Fibers, Preforms, Electronics and Specialty Shapes*; Klein, L. C., Ed.; Noyes Publications: Park Ridge, NJ, 1988; Chapter Antireflective Films from the Sol-Gel Process; pp 80−109.
(4) Nostell, P.; Roos, A.; Karlsson, B. *Thin Solid Films* **1999**, *351*, 170–175.
(5) Bautista, M. C.; Morales, A. *Sol. Energy Mater. Sol. Cells* **2003**, *80*, 217–225.
(6) Cheng, Y.; Wang, Y.; Juang, Y.; O'Neill, M.; Lukas, A.; Karwacki, E.; McGuian, S.; Tang, A.; Wu, C. *J. Phys. Chem. Solids* **2008**, *69*, 518–522.
(7) Grill, A.; Patel, V. *Appl. Phys. Lett.* **2001**, *79*, 803–805.
(8) Milella, A.; Delattre, J. L.; Palumbo, F.; Fracassi, F.; d'Agostino, R. *J. Electrochem. Soc.* **2006**, *153*, F106–F114.
(9) Widodo, J.; Lu, W.; Mhaisalkar, S. G.; Hsia, L. C.; Tan, P. Y.; Shen, L.; Zeng, K. Y. *Thin Solid Films* **2004**, *462−463*, 213–218.
(10) Xi, J.-Q.; Schubert, M. F.; Kim, J. K.; Schubert, E. F.; Chen, M.; Lin, S.-Y.; LiuW; A, S. *Nat. Photon.* **2007**, *1*, 176–179.
(11) Plawsky, J. L.; Kim, J. K.; Schubert, E. F. *Mater. Today* **2009**, *12*, 36–45.
(12) Williford, R.; Fryxell, G.; Li, X.; Addleman, R. *Microporous Mesoporous Mater.* **2005**, *84*, 201–210.
(13) Jo, M.-H.; Hong, J.-K.; Park, H.-H.; Kim, J.-J.; Hyun, S.-H.; Choi, S.-Y. *Thin Solid Films* **1997**, *308−309*, 490–494.
(14) Baney, R. H.; Itoh, M.; Sakakibara, A.; Suzuki, T. *Chem. Rev.* **1995**, *95*, 1409–1430.
(15) Liu, Y. L.; Liu, C. S.; Chen, W. H.; Chen, S. Y.; Wang, K. S.; Hwu, M. J. *J. Nanosci. Nanotechnol.* **2009**, *9*, 1839–1843.
(16) Tao, S.; Yin, J.; Li, G. *J. Mater. Chem.* **2008**, *18*, 4872–4878.
(17) Sel, O.; Sallard, S.; Brezesinski, T.; Rathouský, J.; Dunphy, D.; Collord, A.; Smarsly, B. *Adv. Funct. Mater.* **2007**, *17*, 3241–3250.
(18) Sanchez, C.; Boissière, C.; Grosso, D.; Laberty, C.; Nicole, L. *Chem. Mater.* **2008**, *20*, 682–737.
(19) Besson, S.; Gacoin, T.; Ricolleau, C.; Jacquiod, C.; Boilot, J. P. *J. Mater. Chem.* **2003**, *13*, 404–409.

 Published on Web 03/31/2010

Especially, this has led in the last years to organized mesoporous sol−gel films exhibiting high porosity (up to 60%), which have been suggested as low-k/low-n layers.[20,21] These films are generally synthesized from a mixture containing the classic cetyltrimethylammonium bromide (CTAB) or nonionic polyethylene oxide polypropylene oxide (PEO-PPO) block-copolymer surfactants and a silica sol prepared by acidic hydrolysis of an ethanolic solution of alkoxysilanes, such as the tetraethoxysilane (TEOS).[18,19,22,23] After spin- or dip- coating deposition, the rapid removal of the solvent allows both the micellar organization and its stabilization by gelation of a percolative silica network constituting the wall structure. The organized mesoporous silica films are then obtained after subsequent removal of the micellar template either by calcination for glass substrates or by washing with acetone for plastic substrates. The resulting films present homogeneous distribution of organized mesopores with uniform size (in the 2−10 nm range) separated by highly microporous silica walls leading to a very low value of the refractive index (down to 1.16).

One of the drawbacks of the above-mentioned materials is that their open pore network, constituted of small pores (below 1 nm up to 15 nm), is subject to capillary condensation of atmospheric water which drastically decreases their dielectric properties.[24] Instability of these films is also due to their high specific surface area, which allows a strong adsorption of organic pollutants. To reduce the hydrophilicity of mesoporous thin films, the silica surface has been modified with methyl groups,[25−27] but capillary condensation still occurred because of the very small pore diameter, and the resulting porous films were more sensitive to organic contaminants.[28,29] This suggests, for low-n applications, to decrease the interface of the porous material with its environment, while keeping its porosity constant.

In fact, a strategy to reduce the specific surface area and avoid capillary condensation in porous silica films first consists in the increase of the extrinsic pore size (due to the organic template) up to values corresponding to the frontiers between the meso- and macro range (e.g., typically 30−100 nm).[30] Capillary condensation occurs indeed at relative pressure higher than 0.9 when the pore diameter is increased above 30 nm, as predicted by the Kelvin equation.[31] For such pores sizes, micellar templates cannot be used anymore, and a pre-existing organic sacrificial template such as polymer beads can be envisaged.[32−35] A second important point is to control the intrinsic microporosity in sol−gel silica walls to develop a closed-pore structure, which should significantly limit both water uptake and water adsorption.[36] This implies to avoid high chemical interactions between the silica sol−gel network and the organic template, which are known to inhibit the condensation of silanol groups in organized mesoporous films leading to an open microporosity in silica walls.[37]

In the present study, porous sol−gel silica films were prepared using different PMMA latex nanoparticles of 30−80 nm in diameter as sacrificial templates. First, the organic templates were homogeneously incorporated in the sol−gel silica matrix without aggregation or phase separation. After thermal treatment, the process then led to a sharp pore size distribution similar to the size of the templating latex particles. These extrinsic pores were embedded in a microporous silica network in which the low intrinsic porosity was closed to the ethanol condensation. Consequently, these porous silica films were not subject to capillary condensation of atmospheric pollutants and their porous fraction could be easily tailored in a wide range. We also showed that for porous fractions lower than some percolation threshold of the extrinsic pores, the porosity could be closed (i.e., nonaccessible by moisture from air), leading to highly stable refractive indexes.

Experimental Section

Materials. Tetraethylorthosilicate (TEOS, 98%), methylmethacrylate (MMA, 99%), ammonium persulfate (APS, 98%) were purchased from Aldrich. The anionic surfactant Disponil FES 32 IS was graciously provided by Cognis as a solution of 32 wt % active matter in water. Absolute ethanol (99%) was purchased from Carlo Erba.

Porogen. PMMA latex nanoparticles were prepared by conventional emulsion polymerization of MMA initiated by APS in water, at 70 °C, in a thermostatted reactor under mechanical stirring. Disponil FES 32 IS was used as surfactant. Varying the experimental conditions, three PMMA latex suspensions were prepared with mean diameters of 32, 59, and 77 nm, respectively. The latex particles were characterized both by dynamic light

(20) Saxena, R.; Rodriguez, O.; Cho, W.; Gill, W.; Plawsky, J.; Baklanov, M.; Mogilnikov, K. *J. Non-Cryst. Solids* **2004**, *349*, 189–199.
(21) Bruinsma, P.; Bontha, J. R.; Liu, J.; Baskaran, S. *Mater. Res. Soc. Symp. Proc.* **1997**, *443*, 105–110.
(22) Lu, Y. F.; Ganguli, R.; Drewien, C. A.; Anderson, M. T.; Brinker, C. J.; Gong, W. L.; Guo, Y. X.; Soyez, H.; Dunn, B.; Huang, M. H.; Zink, J. I. *Nature* **1997**, *389*, 364–368.
(23) Grosso, D.; Cagnol, F.; Soler-Illia, G.; Crepaldi, E.; Amenitsch, H.; Brunet-Bruneau, A.; Bourgeois, A.; Sanchez, C. *Adv. Funct. Mater.* **2004**, *14*, 309–322.
(24) Li, Y.; Ciofi, I.; Carbonell, L.; Heylen, N.; Van Aelst, J.; Baklanov, M. R.; Groeseneken, G.; Maex, K.; Tokei, Z. *J. Appl. Phys.* **2008**, *104*, 034113–6.
(25) Jung, S.-B.; Park, H.-H. *Thin Solid Films* **2002**, *420−421*, 503–507.
(26) Xu, Y.; Wu, D.; Sun, Y. H.; Li, Z. H.; Dong, B. Z.; Wu, Z. H. *J. Non-Cryst. Solids* **2005**, *351*, 258–266.
(27) Luo, J.-T.; Wu, W.-F.; Wen, H.-C.; Wan, B.-Z.; Chang, Y.-M.; Chou, C.-P.; Chen, J.-M.; Chen, W.-N. *Thin Solid Films* **2007**, *515*, 7275–7280.
(28) Matheron, M.; Bourgeois, A.; Gacoin, T.; Brunet-Bruneau, A.; Albouy, P.-A.; Boilot, J.-P.; Biteau, J.; Lacan, P. *Thin Solid Films* **2006**, *495*, 175–179.
(29) Balkenende, A.; de Theije, F.; Kriege, J. *Adv. Mater.* **2003**, *15*, 139–143.
(30) Rouquerol, J.; Avnir, D.; Fairbridge, C. W.; Everett, D. H.; Haynes, J. M.; Pernicone, N.; Ramsay, J. D. F.; Sing, K. S. W.; Unger, K. K. *Pure Appl. Chem.* **1994**, *66*, 1739–1758.
(31) Rouquerol, J.; Rouquerol, F.; Sing, K. *Adsorption by Powders and Porous Solids*; Academic Press: New York, 1999.
(32) Falcaro, P.; Malfatti, L.; Kidchob, T.; Giannini, G.; Falqui, A.; Casula, M. F.; Amenitsch, H.; Marmiroli, B.; Grenci, G.; Innocenzi, P. *Chem. Mater.* **2009**, *21*, 2055–2061.
(33) Yacou, C.; Fontaine, M. L.; Ayral, A.; Lacroix-Desmazes, P.; Albouy, P. A.; Julbe, A. *J. Mater. Chem.* **2008**, *18*, 4274–4279.
(34) Julbe, A.; Rouessac, V.; Durand, J.; Ayral, A. *J. Membr. Sci.* **2008**, *316*, 176–185.
(35) DeFriend, K. A.; Barron, A. R. *J. Membr. Sci.* **2003**, *212*, 29–38.
(36) Puyrenier, W.; Rouessac, V.; Broussous, L.; Rébiscoul, D.; Ayral, A. *Microporous Mesoporous Mater.* **2007**, *106*, 40–48.
(37) Ryoo, R.; Jun, S. *J. Phys. Chem. B* **1997**, *101*, 317–320.

scattering (DLS) and scanning electron microscopy (SEM) and showed a monodisperse size distribution with a Gaussian full width at half-maximum less than 10 nm (see Figures S1, S2, and S3 in the Supporting Information).

Porous Silica Films. The silica sol was prepared by mixing 14.2 mL of TEOS (6.4×10^{-2} mol), 11.2 mL of ethanol and 4.62 mL of an HCl solution in deionized water with a pH 2.5. The sol was hydrolyzed at 60 °C under reflux during 1 h corresponding to the complete TEOS hydrolysis, as checked by ^{29}Si NMR spectroscopy. Then 20 mL of the HCl solution was added to the mixture and the ethanol was removed under vacuum. Ethanol was evaporated from the hydrolyzed sol as it might destabilize the latex suspension.[38] The volume of the final solution was adjusted to 22 mL with a pH 2.5 HCl solution to adjust the silicon concentration to 2.90 mol L^{-1}. The residual amount of ethanol was determined to be less than 5 vol % by ^{1}H NMR spectroscopy.

The films were deposited on silicon substrates by spin-coating (2000 rpm, 60s) after mixing of different amounts of silica sol, the latex dispersion and the HCl solution. The silicon wafers were previously cleaned by 15 min immersions in a fresh piranha solution (H_2O_2 (30%)/H_2SO_4 3:1 vol). The latex template was removed by calcination in air at 450 °C for 1h30.

TGA/DTA experiments were performed on the dried latex and on the dried sol. These experiments shown that the latex is fully calcinated above 400 °C, and that the decomposition does not change significantly when the latex is embedded in the sol−gel silica matrix. This was confirmed by FTIR transmission spectroscopy (Figure S4 in the Supporting Information), where the main bands corresponding to PMMA (stretching of CH_2 and CH_3 groups around 2900−3000 cm^{-1}; stretching of the C=O ester double bond at 1730 cm^{-1}) are no more present on the spectrum when the films are cured at 400 °C or higher.

Characterization. Average size and size distribution of the latex particles were investigated by dynamic light scattering on a Malvern Zeta Sizer. The autocorrelation function was fitted assuming a monomodal Gaussian distribution of particle size.

Thickness and porous fraction of the porous silica films were determined by spectroscopic ellipsometry in the visible range (1.5−4.7 eV) at an incidence angle of 70°. Data were processed using a Bruggeman effective medium approximation between dense fused silica and vacuum. Note that using this optical model, a pure sol−gel silica film (without latex) cured at 450 °C is measured to have an intrinsic porous fraction around 5−10% because of its density being lower than the fused silica.

Ellipsometry−porosimetry experiments were performed in a home-built temperature-controlled vacuum cell, which was adapted on a visible spectroscopic ellipsometer for in situ measurements at an incidence angle of 75°. The ethanol vapor pressure was progressively increased to measure the adsorption. At each step of the sorption process, in situ visible ellipsometric measurements were performed to evaluate the thickness and the refractive index of films.[39,40]

Infrared spectra of the films deposited on silicon were recorded on a Thermo Nicolet FTIR spectrometer Nexus. Each spectrum was recorded in transmission mode between 650 and 4000 cm^{-1}.

Direct observations of film cross-section and film surface were performed by Field Effect gun scanning electron microscopy (FE-SEM) and by atomic force microscopy (AFM, tapping mode), respectively.

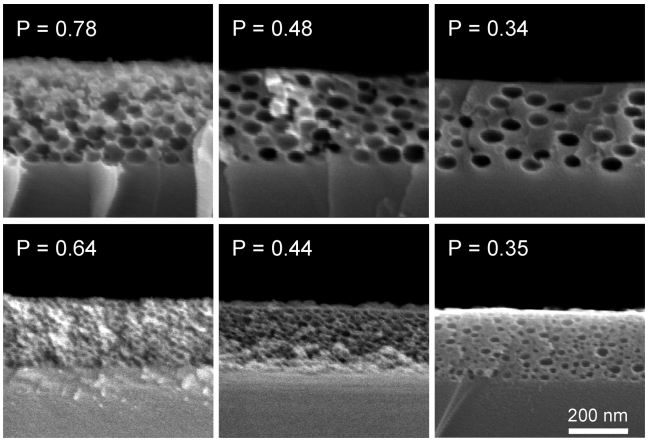

Figure 1. SEM pictures of porous thin films with equivalent porous fraction, but with pore size of 77 nm (top) and 32 nm (bottom). For all the films, the solid content C is kept constant at 15%.

Nanoindentation tests were investigated by using an instrumented nanoindenter XP (MTS) with a Berkovich tip on films of 1 μm thick. Methodology is described elsewhere.[41]

Results

Porous silica thin films were prepared through a conventional sol−gel process under various experimental conditions. As shown in the SEM cross-section observations (Figure 1), the films exhibit a network of pores whose size and shape are comparable to those of the latex templates. Pores are disordered and homogeneously dispersed.

The film thickness and the porous fraction were tailored by varying two parameters C and P defined as follows:

$$C = \frac{m_{SiO_2} + m_{PMMA}}{m_{sol}} P = \frac{V_{PMMA}}{V_{SiO_2} + V_{PMMA}}$$

Where m_{SiO_2} and m_{PMMA} are the corresponding masses of silica and PMMA related to the silicon concentration and the polymer content in the solution (total mass m_{sol}). m_{SiO_2} is taken as the product of the TEOS molar content by the silica molar mass. V_{SiO_2} and V_{PMMA} are the corresponding volumes of the silica and PMMA phases determined from their mass taking their respective densities equal to 2.20 (fused silica) and 1.18.

The C parameter is the non volatile mass content of the sol, further abbreviated as the solid content. The P parameter corresponds to the volume fraction of polymer beads in the final silicated composite, further abbreviated as the latex volume fraction.

Using spectroscopic ellipsometry measurements and as previously observed,[42] the experimental evolution of the film thickness was shown to linearly scale with the solid content C of the sol keeping constant the latex volume fraction (Figure 2a). The porous fraction was deduced

(38) Odriozola, G.; Schmitt, A.; Callejas-Fernández, J.; Hidalgo-Álvarez, R. *J. Colloid Interface Sci.* **2007**, *310*, 471–480.
(39) Baklanov, M. R.; Mogilnikov, K. P. *Microelectron. Eng.* **2002**, *64*, 335–349.
(40) Brunet-Bruneau, A.; Besson, S.; Gacoin, T.; Boilot, J. P.; Rivory, J. *Thin Solid Films* **2004**, *447−448*, 51–55.
(41) Chemin, N.; Rozes, L.; C, C.; Cassaignon, S.; Bourhis, E. L.; Jolivet, J.-P.; Spalla, O.; Barthel, E.; Sanchez, C. *Chem. Mater.* **2008**, *20*, 4602–4611.
(42) Meyerhofer, D. *J. Appl. Phys.* **1978**, *49*, 3993–3997.

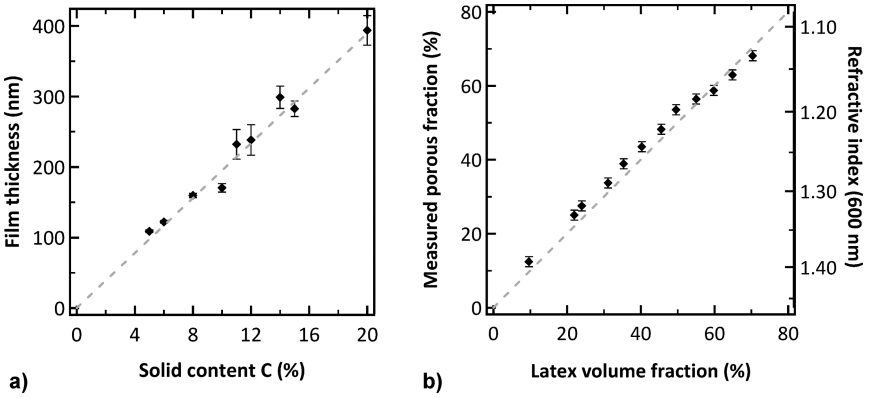

Figure 2. (a) Evolution of the film thickness measured by ellipsometry with the solid content C keeping constant the latex volume fraction P at 50%; (b) evolution of the porous fraction measured by ellipsometry with the calculated latex volume fraction P with a C parameter kept constant at 10%.

from ellipsometry experiments by considering the silica network as dense fused silica (see Experimental Section). This allowed observing that the latex volume fraction P parameter was very close to the porous fraction in the silica film after calcination (Figure 2b). Consequently, the refractive index of the film could be tuned from 1.10 to 1.45 by changing the P value.

The relatively low microporosity of silica walls was also confirmed by FTIR experiments (see Figure S4 in the Supporting Information). By increasing the curing temperature of films, a progressive decrease of intensity is observed for the Si−OH stretching band (950 cm^{-1}) and for the hydroxyl stretching band (3000 cm^{-1}). However, as expected for a sol−gel silica film, a fraction of silanol groups remain after heating at 450 °C, suggesting that a few percent of microporosity subsist in silica walls. Note also at 450 °C the very low intensity of the band at 3000 cm^{-1} showing a weak quantity of absorbed water on the silica surface.

SEM cross-sections also clearly show that by keeping the solid content C constant and varying the polymer content P, it was possible to tailor the porosity (pore size and porous fraction) independently of the film thickness (Figure 1).

The surface of porous thin films was observed by AFM microscopy (Figure 3). On the whole porous fraction range, pores are seen to be open on the surface. A ring is often observed around the surface pore probably due to some wetting of the latex beads by the silica sol (scheme Figure 3). The measured surface roughness (rms) of the films is between 1 and 2 nm (as the microscope tip does not probe the depth of the surface pores). The images show a fluctuation of the mean surface height with amplitude lower than 7 nm.

The pore structure was investigated by ellipsometry−porosimetry.[39,40] Ethanol adsorption isotherms were measured on films with various porous fractions and various pore diameters ranging from 30 to 80 nm. An example of the obtained isotherms is displayed in Figure 4 for films with similar porous fraction (around 0.5) and various pore diameters. In comparison, an isotherm was also measured on a CTAB -templated mesoporous silica film with a 3D hexagonal pore structure containing an

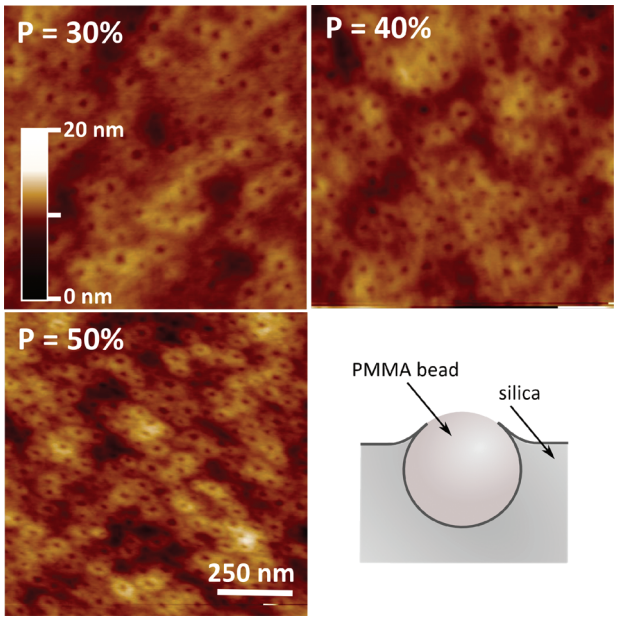

Figure 3. AFM images of the surface topology of porous silica films with various porous fractions. At the bottom on the right, scheme of the wetting of the bead by silica.

extrinsic mesopore fraction of 0.33 (pore diameter of 4 nm)[28] and an intrinsic micropore fraction of 0.22 (open pores in silica walls with a diameter less than 2 nm).[43]

A first expected observation is that the effect of adsorption on the refractive index significantly decreases when the extrinsic pore size increases, as the specific surface area scales inversely with the pore diameter. More precisely, adsorption due to the existence of an open microporosity in silica walls should be observed in the low partial pressure range ($P/P_0 < 0.10$). This is the case for the 3D-hexagonal mesoporous sample, with a strong ethanol adsorption for relative partial pressures under 0.10, in contrast with the films with pore sizes bigger than 30 nm.

For higher ethanol partial pressures, capillary condensation can occur and the position of this phenomenon is

(43) Sing, K. S. W.; Everett, D. H.; Haul, R.; Moscou, L.; Pierotti, R.; Rouquerol, J.; Siemieniewska, T. *Pure Appl. Chem.* **1985**, *57*, 603–619.

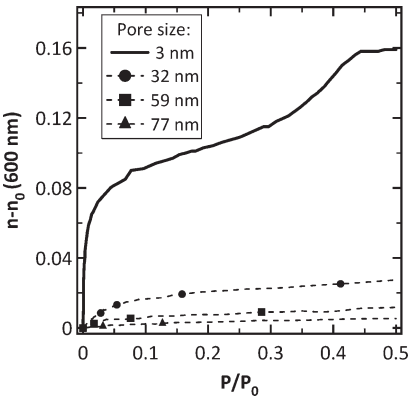

Figure 4. Ethanol adsorption isotherms in porous silica films with porous fraction around 0.50. Full line, mesoporous film templated with CTAB; dotted lines, porous films templated with 32 nm (●), 59 nm (■), and 77 nm (▲) latex particles.

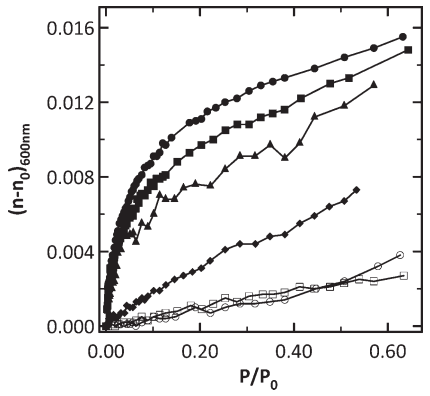

Figure 5. Adsorption isotherms measured on porous thin films with different porous fractions (● 0.69, ■ 0.60, ▲ 0.53, ♦ 0.45, ○ 0.37, □ 0.29) prepared with a 59 nm diameter latex suspension.

directly linked to the pore diameter through the Kelvin's equation.[31] For the mesoporous sample (pore radius 2 nm), the capillary condensation takes place in mesopores around $P/P_0 = 0.4$ (Kelvin radius of 1.6 nm). This contrasts with the absence of capillary condensation observed in latex templated films as the Kelvin radius for ethanol capillary condensation in silica is 16 nm for a relative pressure of 0.9.

The effect of the porous fraction on adsorption isotherms was investigated for the three pore sizes (an example is shown in Figure 5 for a pore size of 59 nm). The evolution is similar for the three pore sizes with an abrupt transition in the general shape of the isotherms when varying the porous fraction. In the high porous fraction range (e.g., above 0.50), the isotherms are of type II,[43] i.e., characteristic of the adsorption on a plane surface or in macropores, whereas for a porous fraction below 0.50, the isotherms indicate a very low adsorption.

Desorption isotherms were also recorded on our films and showed, as expected, that the adsorption process was perfectly reversible, as no capillary condensation phenomenon occurred. Note also that no significant kinetics effect was detected during the adsorption, as no change in the refractive index was measured by maintaining a partial pressure ($P/P_0 = 0.4$) for an hour in the measurement cell.

Discussion

The latex-templated porous silica films described above have a homogeneous disordered porosity. Contrary to surfactant-templated films for which the pore structure is know to drastically evolve with the surfactant/silica ratio,[19,44] the use of latex beads as sacrificial porogen allowed us to prepare films in a wide porous fraction range (from 0.10 to 0.74) keeping structure and keeping a constant thickness.

The strong adsorption observed at low pressure in mesoporous CTAB-templated silica films was previously attributed to condensation in micropores existing in the silica walls.[28,45] In contrast, it seems that silica walls of latex-templated films present a low microporosity closed to the ethanol condensation as, first, the measured porous fraction is very close to the latex volume fraction (Figure 2b), and, second, the increase of the refractive index in the low partial pressure range is moderate. This could be due to weaker interactions between the condensing nucleophilic silica with the anionic surfactant covering the latex particle surface when compared to the cationic CTAB micelles.[37] The high electrostatic and chemical interactions between micelle templates and silanol groups are well-known to be at the origin of the mesostructuration of silica films implying highly porous silica network in the walls. Obviously, as observed on FTIR spectra, some dangling Si−OH bonds remain in the latex-templated films cured at 450 °C, but the resulting free space in silica walls seems to be closed to the ethanol adsorption.

For a fine analysis of adsorption data, they were plotted as t-plots,[31] where the volume fraction of ethanol adsorbed in the porous films is plotted against the thickness t of ethanol adsorbed on a flat surface. The adsorption layer thickness of ethanol on hydrophilic native oxide on silicon cured for 1 h 30 min at 450 °C was taken as reference, to ensure a surface chemistry as close as possible to the one of sol−gel silica cured at 450 °C.[43] Linear parts in the t-plot correspond to adsorption on flat surfaces, the slope giving access to the specific surface area in $m^2\,cm^{-3}$. Note that no confinement effect should interfere with the t-plot as the pore size is sufficiently high.[46]

From a geometrical point of view, assuming that extrinsic pores are spherical, the specific surface area is given by the relationship

$$S_{\text{area}} = \frac{S_{\text{PMMA}}}{V_{\text{SiO}_2} + V_{\text{PMMA}}} = \frac{3}{r_{\text{PMMA}}} \frac{V_{\text{PMMA}}}{V_{\text{SiO}_2} + V_{\text{PMMA}}} = 3\frac{P}{r_{\text{PMMA}}}$$

, where r_{PMMA} is the radius of the PMMA beads, and S_{PMMA} is their surface.

Three representative t-plots for adsorption in films with porous fraction around 0.50 and pore size from 32 to 77 nm are plotted in Figure 6. All three curves are linear with a very low intercept showing that the beginning of the adsorption is equivalent to the adsorption on a flat surface with no condensation phenomenon. This is another confirmation

(44) Jung, S.-B.; Ha, T.-J.; Seon, J.-B.; Park, H.-H. *Microporous Mesoporous Mater.* **2008**, *111*, 188–193.
(45) Bourgeois, A.; Brunet Bruneau, A.; Fisson, S.; Demarets, B.; Grosso, D.; Cagnol, F.; Sanchez, C.; Rivory, J. *Thin Solid Films* **2004**, *447−448*, 46–50.
(46) Kruk, M.; Jaroniec, M. *J. Phys. Chem. B* **2002**, *106*, 4732–4739.

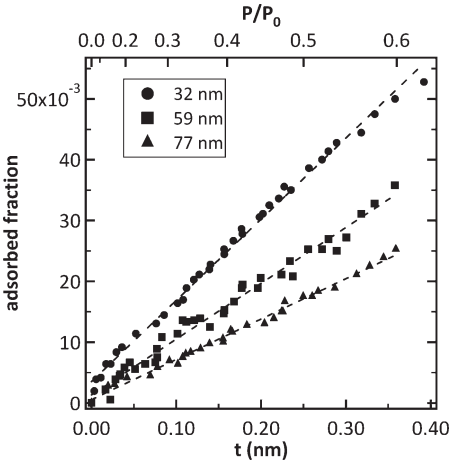

Figure 6. *T*-plot for the adsorption in thin films with porous fraction around 0.50 and prepared with a 32 nm (●), 59 nm (■), or 77 nm (▲) diameter latex template, and linear fit in dotted line. The corresponding partial pressures are reported on the top axis.

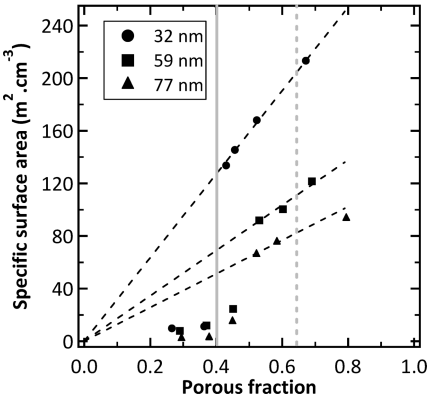

Figure 7. Evolution of the relative specific surface area with the porous fraction for three different porogen sizes (▲77 nm, ■59 nm, ● 32 nm). Dotted black lines represent the theoretical linear evolution of specific surface area with porous fraction. The gray vertical full line represents the porous fraction threshold between open and closed pore structure, whereas the dotted vertical line represents the random closed packing (RCP) percolation threshold.

of the absence of microporosity accessible to ethanol in the latex templated films. Regarding the slopes corresponding to 32, 59, and 77 nm pore size, the measured specific surface areas were (geometrical expected value) 168 (98), 92 (54) and 67 (41) m^2/cm^3 respectively. The ratio between the experimental and expected values is constant and equal to 1.7. The discrepancy between the geometrical and experimental specific surface area can arise from uncertainty in the model (pores are spheroïdal) but other origins such as some roughness of the pore surface or difference in the surface chemistry in comparison to the model surface cannot be discarded.

The evolution of the t-plot specific surface area with the porous fraction (in the range 0.20 to 0.75) is shown in Figure 7 for the three pore sizes. A sharp increase in specific surface area was observed around porous fractions of 0.40−0.45. Note that the threshold is approximately the same for the three porogen sizes. Above the threshold, the specific surface area evolved linearly whatever the porogen size. Moreover, the ratio between the slopes is equal to the ratios between porogen sizes, as expected from the above-mentioned geometrical model. Below the threshold, almost no evolution of the specific surface area was detected, and this area was very low. This can be interpreted as a transition between a closed pore structure to the ethanol vapor adsorption and an open one where the specific surface area fits with geometry.

The position of the threshold can be discussed in the light of random packing of spheres and percolation theory.[47] Equilibrium random packing of spheres leads to a percolation threshold of 0.64,[48] which is significantly higher than the observed one. Theoretical results can help understanding this discrepancy. Even if the process of film deposition by spin-coating is out of equilibrium, the repulsive electrostatic forces between the particles ensure the packing to be close to equilibrium. The small thickness of the film relative to the pore diameter could lower the position of the threshold (finite size scaling), however by dividing the pore size by two, the gap between the theoretical and experimental threshold should scale the same way, which is not the case.[49] A more convincing explanation could be that some limited aggregation of the PMMA particles occurs during spin-coating. This can be formalized by considering a soft penetrable shell around particles which allows contact between one another despite the electrostatic repulsion. In a so-called Cherry-Pit model, a soft shell as thin as 10% of the sphere diameter can lower the threshold down to 0.40.[47]

Conclusion

A series of monodisperses PMMA latex particles, with diameters in the range 30−80 nm, have been synthesized and used as templates for the elaboration of porous sol−gel silica films. Changing the size and the concentration of the latex particles in the deposited sol enabled us to tailor the porosity (pore size and porous fraction) independently of the film thickness.

An important point is that contrary to what is commonly observed in surfactant templated systems, we note the absence of an important microporosity in the silica network as shown by the correspondence between the measured porous fraction after calcination and the initial latex volume fraction. As a first consequence, it was possible to prepare films with the same thickness, exhibiting different concentrations of uniform extrinsic pores (porous fraction from 0.10 to 0.74) separated by closed microporous silica walls. A second consequence is that no capillary condensation occurred in these films before high partial pressure (above 0.9), as shown from ethanol adsorption isotherms. This led to films presenting a low refractive index that can be tuned in a large range (from 1.10 to 1.45 at 600 nm).

It can be expected that the stability of films against the water adsorption is not significantly modified compared

(47) Torquato, S. *Random Heterogeneous Materials − Microstructure and Macroscopic Properties*; Springer-Verlag: New York, 2002.
(48) Berryman, J. G. *Phys. Rev. A* **1983**, *27*, 1053–1061.
(49) Wagner, N.; Balberg, I.; Klein, D. *Phys. Rev. E.* **2006**, *74*, 011127.

Table 1. Measured Refractive Index of Porous Films with Various Porous Fractions and/or Templates in Ambient Condition (RH 60%, atmospheric pressure), in Vacuum (under 10^{-6} Torr, in the ellispometry-porosimetry cell), and after Aging for 15 Months in Ambient Conditions[a]

template	porous fraction	n (600 nm) (RH = 60%)	n (600 nm) ($\times 10^{-6}$ Torr)	n (600 nm) 15 months later
latex 60 nm	0.20	1.327 ± 0.003	1.325 ± 0.003	1.367 ± 0.003
latex 60 nm	0.40	1.254 ± 0.003	1.251 ± 0.003	1.287 ± 0.003
latex 60 nm	0.70	1.145 ± 0.003	1.142 ± 0.003	1.167 ± 0.003
CTAB	around 0.40	1.401 ± 0.003	1.270 ± 0.003	

[a] In the last case, the original optical properties are recovered after rinsing the films with ethanol and acetone.

to the one observed during the ethanol adsorption as, taking into account the Kelvin relation, the water capillary condensation should be also observed above a partial pressure of 0.9. A clear confirmation of this stability is shown in Table 1, where the refractive index measured on latex templated-films is the same under vacuum and at 60% relative humidity. Moreover, the refractive index is shown to be stable over months in ambient conditions, thanks to the low specific surface area. It can be also noted that the original optical properties of films are restored by a simple rinsing treatment with ethanol and acetone. This behavior drastically contrasts with the one observed for organized mesoporous silica films prepared from surfactant templates which do not present stable dielectric properties under ambient atmosphere due to capillary condensation occurring within their small sized micro- and mesopores (5−10 nm).

Another noteworthy result concerns the drastic change of the relative specific surface area (as determined from the t-plot analysis), observed for a porous fraction of about 0.40 for different sizes of the initial template. This probably corresponds to a porosity percolation transition with the opening of the extrinsic pore interconnection. The closed porosity structure was observed for highly stable films with a low refractive index of 1.29 at 600 nm, which is promising for antireflective applications.

Concerning this closed porosity structure, one may wonder how the latex combustion products diffuse through the disconnected extrinsic pores during the calcination. In fact, the thermal decomposition of the latex between 300 and 400 °C produces gaseous CO_2 and H_2O[50] that may diffuse through the not yet fully condensed silica network. The detection of a closed pore structure from adsorption measurements suggests that the path followed by the combustion products may be progressively closed by the pursuing silica condensation, evidenced in the 400−500 °C range by FTIR spectroscopy (see Figure S4 in the Supporting Information).

(50) Dakka, S. *J. Therm. Anal. Calorim.* **2003**, *74*, 729–734.

Table 2. Young's Modulus of 60 nm Latex Templated Films Measured by Nanoindentation on 1 μm Thick Films, Compared to Literature Results Obtained on Mesoporous Films with Various Organization of the Porosity[51]

porous fraction	Young's modulus (GPa) of 1 μm thick 60 nm latex templated films	Young's modulus (GPa) range obtained for mesoporous films[51]
0.35	19 ± 1	15−19
0.45	13 ± 1	11−17
0.50	11 ± 1	9−16

More generally, it is clear that all the characteristics of these new porous silica films markedly improve the reliability and performance of sol−gel coatings for applications in optics and microelectronics. However, one of the main drawbacks with very porous thin films is their mechanical properties that can be significantly altered with the increase in porous fraction.[52] Preliminary nanoindentation results performed on latex templated films (Table 2) are in a good agreement with data obtained on mesoporous films with ordered or disordered porosity.[51] These mechanical data tend to show that although the Young's modulus is naturally decreased when the porous fraction increases, no drastic change in the mechanical properties is observed by passing through the percolation threshold. Further experiments are in progress to characterize more precisely the scaling of the mechanical properties of the porous films described above, on the whole porous fraction range.

Acknowledgment. F.G. deeply acknowledges Saint-Gobain for financial support and A. Lelarge for SEM pictures. The authors thank F. Devreux, P. Levitz, J. Teisseire, and N. Chemin for fruitful discussions.

Supporting Information Available: SEM pictures and size distribution of the PMMA latex particles (PDF). This material is available free of charge via the Internet at http://pubs.acs.org/

(51) Fan, H.; Hartshorn, C.; Buchheit, T.; Tallant, D.; Assink, R.; Simpson, R.; Kissel, D. J.; Lacks, D. J.; Torquato, S.; Brinker, C. J. *Nat. Mater.* **2007**, *6*, 418–423.

(52) Volinsky, A. A.; Vella, J. B.; Gerberich, W. W. *Thin Solid Films* **2003**, *429*, 201–210.